Journal of
Synchrotron Radiation

ISSN 0909-0495

Received 16 May 2007
Accepted 20 June 2007

XAS and XMCD under high magnetic field and low temperature on the energy-dispersive beamline of the ESRF

O. Mathon,[a]* P. van der Linden,[a] T. Neisius,[b] M. Sikora,[a] J. M. Michalik,[c] C. Ponchut,[a] J. M. De Teresa[d] and S. Pascarelli[a]

[a]European Synchrotron Radiation Facility, BP 220, 38043 Grenoble CEDEX, France, [b]CP2M, Université Paul Cézanne, 13397 Marseille CEDEX 20, France, [c]Department of Solid State Physics, Faculty of Physics and Applied Computer Science, AGH University of Science and Technology, 30-059 Krakow, Poland, and [d]Instituto de Ciencia de Materiales de Aragón, Universidad de Zaragoza-CSIC, Facultad de Ciencias, 50009 Zaragoza, Spain. E-mail: mathon@esrf.fr

The present paper demonstrates the feasibility of X-ray absorption spectroscopy (XAS) and X-ray magnetic circular dichroism (XMCD) under high magnetic fields up to 26 T and low temperatures down to 5 K on the ID24 energy-dispersive XAS beamline of the ESRF. The pulsed magnetic field set-up, entirely developed at the ESRF, is described as well as the beamline set-up, the synchronization and the measurement procedure. It allows field strengths up to 30 T. Finally, as an example, we report a recent XMCD study at the Re L_2 and L_3 absorption edges of the double perovskite Sr_2CrReO_6.

Keywords: pulsed magnetic fields; X-ray magnetic circular dichroism; X-ray absorption spectroscopy; energy-dispersive optics.

1. Introduction

Considerable efforts in present research are made to understand properties of matter under extreme conditions. For example, static high pressures up to the multimegabar regime can be reached with diamond-anvil cells, as well as temperatures from the milli-Kelvin to thousands of Kelvin using dilution refrigerators and laser heating. The exploration of these wide P–T diagrams has lead to the discovery of a multitude of new chemical and physical phenomena, leading to fundamental understanding as well as technological applications. Studies of materials under extreme magnetic fields have the same potential impact. Applying high magnetic fields leads to a variety of phenomena like, for example, structural or magnetic phase transitions or to the discovery of previously unexplored quantum critical points.

Standard split-pair static magnetic fields given by superconductors for synchrotron use are usually limited to 8 T. Split-pair superconductor or resistive magnets can reach static magnetic fields in the 15–20 T range. They are now available or under development at large neutron or X-ray facilities. Specialized high-field laboratories can generate static fields up to 40 T at the expense of tens of megawatts of DC power. An alternative solution calls for the production of pulsed magnetic fields. These allow even higher values to be reached, up to 60 T in a non-destructive mode, for moderate costs in terms of equipment and financial resources. The experimental techniques available at high-magnetic-field research facilities are limited to measurements of macroscopic properties, such as thermal conductivity, resistance, heat capacity, total magnetization or relative changes in lattice parameters through magnetostriction, for example. However, it has recently become possible to transport this kind of instrumentation to large facilities such as synchrotrons, where microscopic properties can be probed. For practical reasons these studies are presently limited to fields up to 40–50 T, for which the required power supplies, although bulky, are transportable.

The time profile of such magnetic field pulses, typically from 0.1 to 50 ms, is suited to typical integration times used at third-generation synchrotron facilities. Consequently, the combination of synchrotron experiments with pulsed high magnetic fields has led to interesting achievements mainly using X-ray diffraction (Matsuda *et al.*, 2004; Frings *et al.*, 2006; Narumi *et al.*, 2006).

We present in this paper, for the first time to our knowledge, an X-ray magnetic circular dichroism (XMCD) study under pulsed high magnetic fields. XMCD is the difference between X-ray absorption spectra obtained with right-handed and left-handed circular polarization. For a finite XMCD signal to be measured, the sample must present a net ferromagnetic or ferrimagnetic moment. The XMCD signal is then directly proportional to the magnetic moment on the absorber atom. Furthermore, under certain conditions, it is possible using the sum rules to derive the amplitude of both the spin and the orbital magnetic moments of the probed atom (Thole *et al.*,

1992; Altarelli, 1993; Carra *et al.*, 1993; Ankudinov & Rehr, 1995). Owing to its element and orbital selectivity, XMCD has been widely used as a very useful probe of magnetic properties (for a recent review, see *e.g.* Stöhr, 1999). In the hard X-ray regime, owing to the higher penetration depth of the photons, it has the additional advantage of being bulk sensitive. In addition to the sensitivity to the magnetic moment of the dichroic signal, the associated average XAS spectrum contains information on the electronic and local structure. Thus, an XMCD experiment gives access to simultaneous information on the magnetic moment on the absorber atom, as well as its local structural and electronic properties.

The XMCD measurements were recorded on the energy-dispersive XAS beamline ID24 of the ESRF. The dispersive set-up allows the whole energy range of the XMCD/XAS spectrum to be recorded in parallel. This is crucial for measurements under high magnetic fields in pulsed mode as the lifetime of the coil limits drastically the number of possible measurement cycles.

In the next section we give a description of the pulsed magnetic field set-up developed by the ESRF. In §3 we briefly describe the experimental layout for XMCD experiments under pulsed magnetic fields on the energy-dispersive beamline ID24, with emphasis on the detection and synchronization aspects. Finally, in §4 we report a recent XMCD study at the Re L_2 and L_3 absorption edges of the double perovskite Sr_2CrReO_6.

2. ESRF pulsed magnetic field set-up

2.1. General description

The set-up was entirely developed by the sample environment group of the ESRF. It consists of a coil with its cryostat and of an independent sample cryostat. A photograph of the set-up is presented in Fig. 1. This system was designed and optimized for synchrotron high-energy X-ray measurements. The compact dimensions (around 20 cm × 20 cm × 30 cm) and weight (less than 8 kg) of the system make it transportable from one beamline to another. The system is compatible with many measurement techniques like diffraction, nuclear scattering or, in this case, XAS/XMCD in the energy-dispersive mode. The field can be applied either parallel or perpendicular to the X-ray propagation direction. In the case of XMCD, the magnetic field is applied parallel to the X-ray path.

2.2. Coil design and magnetic field performance

The simple solenoid coil has a size of 30 mm for the outer diameter with a bore diameter of 11 mm and a length of 20 mm. The coils are wound in-house and the mounting system allows for very fast replacement. The coil is immersed in a bath of liquid nitrogen arriving continuously into the cryostat through a siphon. The coil holder is constructed in such a way that the coil bore is under vacuum and isolates the coil cryostat from the sample cryostat. Consequently the X-ray beam does not pass through the nitrogen bath. Samples of maximum diameter 3 mm can be mounted on the sample holder, which is then inserted inside the magnet bore. A complete description of the system can be found elsewhere (van der Linden *et al.*, 2007).

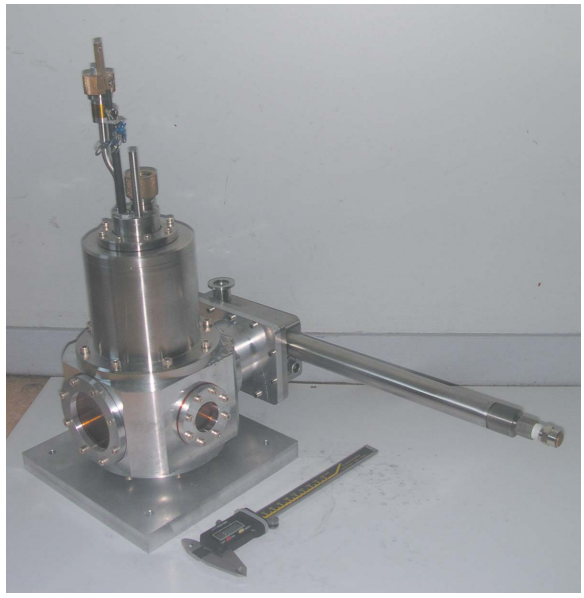

Figure 1
Overview of the ESRF set-up for high magnetic fields and low temperatures.

The coil design is one of the key parameters to gain for example in terms of duty cycle and maximum field reachable. The monolithic coil is wound of 1.2 mm × 1.6 mm Cu (+0.08% Ag) wire. The six layers are wet wound with blue stycast 2850FT and the isolation between the layers was improved by a 0.1 mm layer of glass fiber tissue. This leads to a 30 mH inductance and a resistance at 77 K of about 10 mΩ. The coil is powered by a commercially available capacitor bank (METIS CDMM4kJ3kV capacitive discharge magnetizer) of 4 kJ, 3 kV and 1 mF. The power supply allows positive or negative pulses to be produced, triggered by a TTL signal or driven by a RS232 link. The total resistance of the system, including the coaxial current lead and the fixation loss, amounts to 70 mΩ.

Charging the power supply up to 2500 V yields magnetic pulses of 26 T absorbing about 2 kJ into the coil. Two pick-up coils are installed at the edge of the coil on the cryostat tail. The pick-up voltage dB/dt is used for the field characterization. The total duration of the half-sine-shaped pulse is 650 µs with a slight deformation of the decreasing part owing to resistive coil heating during the pulse. A reproducibility of better than 1 µs of the shape and of the rise time was observed throughout the experiment with a variation of less than 2% of the maximum field.

The temperature of the coil after each pulse was measured using a Pt100 gauge close to the inner windings. When the temperature reached a pre-defined value of 110 K, the next measurement cycle was started. This leads to a repetition rate of one shot per 90 s at 26 T. During one week of experiment, a total of about 5×10^4 pulses (at different field strengths) have been performed without damaging the coil. A typical pulse is shown in Fig. 2.

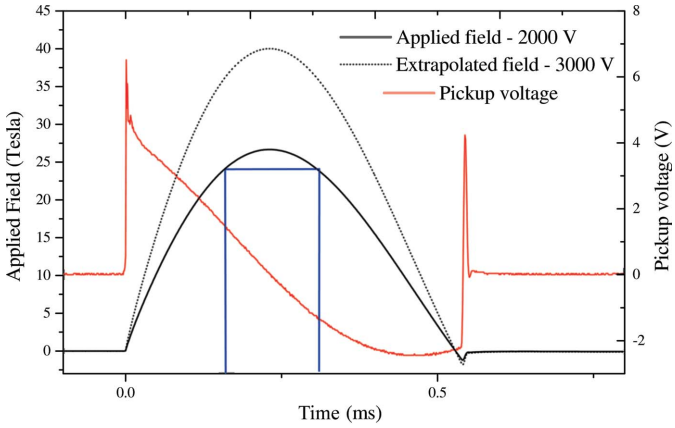

Figure 2
Performance of the ESRF pulsed magnetic field set-up. The rectangle defines a typical integration window measurement.

We found that the repetition rate can be increased by a factor of three if the cooling temperature of the pre-defined coil is set to 200 K. A new coil design consisting of two coaxial coils with cooling slit in between has demonstrated an increase by a factor of ten of the repetition rate (van der Linden *et al.*, 2007) at 26 T (charging at 2000 V).

2.3. Sample cryostat

One of the main advantages of this system is that the cooling of the sample is independent of the cooling of the coil. A small He flux cryostat is inserted inside the coil. He is passed through a heat exchanger located 40 mm in front of the sample. A heater and a temperature gauge allow control of the temperature at ± 0.01 K *via* a Lakeshore temperature controller. The sample is mounted directly in the continuous He flow stream. This system allows a thermalization of the sample independently of the heat capacity of the sample. This is very important, for example, for XAS measurements where powder samples are often used and are difficult to cool down. The sample holder is inserted and removed from the cryostat, allowing fast and simple sample change. The sample is fixed with a threaded cap. Details of the cryostat system and the sample holder are presented in Fig. 3. It allows temperature measurements from 5 K up to room temperature independently of the coil temperature. This is a great advantage for temperature-dependent measurements but also to improve the duty cycle of the coil.

3. Set-up of the energy-dispersive XAS beamline ID24 for high-magnetic-field experiments

3.1. Introduction

Beamline ID24 is the ESRF XAS beamline with parallel detection of the whole spectrum made possible by energy-dispersive highly focusing X-ray optics. The absorption spectrometer is coupled to three low-K undulators in a high-β section of the ring, through a Kirkpatrick–Baez optical system. The energy range of operation is 5–27 keV. The spectral characteristics required for experiments at selected absorption edges are obtained by gap tuning and tapering the undulators. The original and the recently upgraded design of the beamline can be found elsewhere (Hagelstein *et al.*, 1993, 1997; Pascarelli *et al.*, 2004).

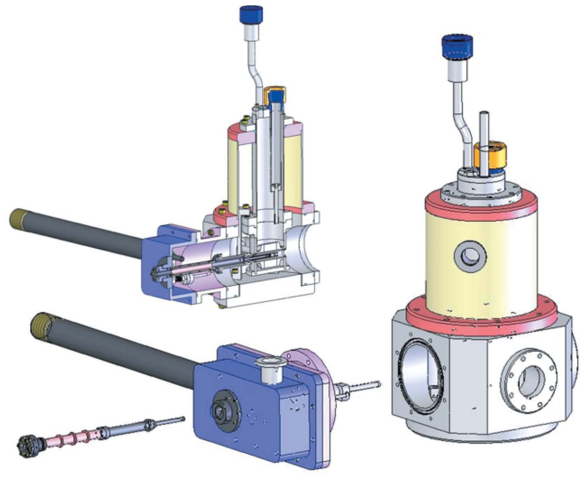

Figure 3
Exploded view of the high-magnetic-field and cryostat set-up. From left to right: sample holder, independent sample cryostat and high-magnetic-field vessel. The X-ray beam passes collinearly to the direction of the exploded view axes. A cross-section view of the set-up is shown in the top left-hand corner.

This beamline is particularly suited for XMCD and XAS measurements under pulsed high magnetic fields. The undulator source, the parallel acquisition of the spectra and the focusing optical scheme of the beamline allow the following necessary requirements to be covered for high-magnetic-field XMCD experiments.

(i) A small focal spot allows the dimensions of the coil to be reduced. The undulator beam on ID24 undergoes double focusing in both directions, and its dimensions, in the 5–25 keV energy range, are below 100 µm. This also allows micro-coil applications already used on ID24 (Bonfim *et al.*, 1998; Mackay *et al.*, 2000).

(ii) A stable beam. The required signal-to-noise ratio is obtained by averaging a large number of spectra. During the acquisition of a series of spectra to be averaged, the beam has to have excellent spectral and spatial stability. This is possible owing to the dispersive optics scheme.

(iii) Fast acquisition. Owing to the in-house development of the detector and of a fast gating system, it is possible to integrate only during the maximum of the magnetic pulse (*i.e.* 150 µs).

(iv) High flux. To compensate for the small integration time and to reach the required signal-to-noise level, the highest flux possible is needed.

3.2. Optical scheme

Fig. 4 illustrates the present optical scheme for high-magnetic-field measurements. It consists of a pair of mirrors in a Kirkpatrick–Baez (KB) geometry, a Si(111) polychromator, a diamond quarter-wave plate (QWP), an optional third vertically refocusing mirror, the sample environment (coil, coil

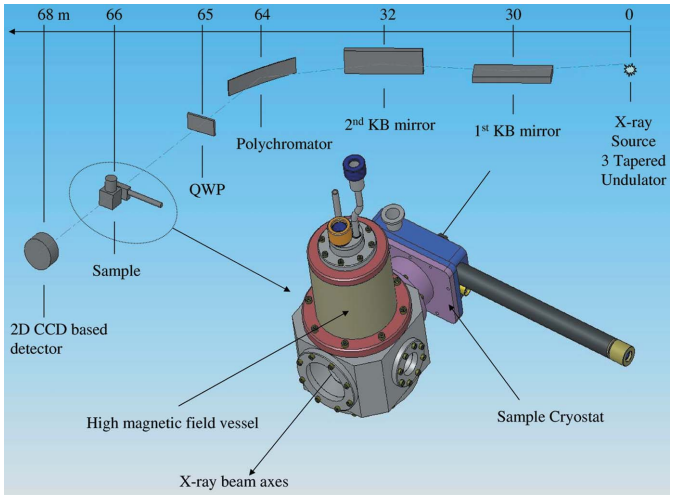

Figure 4
ID24 optical scheme and sample environment for XMCD under high magnetic field (not scaled).

cryostat and sample cryostat) and a position-sensitive detector that transforms the energy–direction correlation into an energy–position correlation (Koch *et al.*, 1995). Additional details of the standard optical set-up may be found by Hagelstein *et al.* (1997), Pellicer-Porres *et al.* (1998), San-Miguel *et al.* (1998) and Pascarelli *et al.* (2004).

The polychromator is located at 64 m from the source. The quarter-wave plate is located 750 mm downstream from the polychromator. Depending on the working energy, it consists of a thin perfect diamond (low energy) or silicon (high energy) crystal in the Laue geometry. Its birefringence properties close to a Bragg reflection transform the linearly polarized incident X-ray beam into a transmitted (non-deviated) beam with circular polarization very close to unity (Giles *et al.*, 1994). The very small source divergence and the non-dispersivity condition allow circular polarization close to unity to be obtained on the whole polychromatic and divergent fan (Pizzini *et al.*, 1998). XMCD applications on ID24 currently cover a wide energy range that extends from the L edges of rare earths (down to the L_3 edge of Ce at 5.7 keV) up to the L edges of 5*d* metals and 4*f* actinides (tested up to the L_3 edge of U at 17.166 keV). Beamline ID24 has a solid experience of XMCD under extreme conditions of pressure (Mathon *et al.*, 2004*a*,*b*) and pressure and temperature (Trapananti *et al.*, 2007).

3.3. Detection

Pseudo time-resolved experiments are carried out using the same stroboscopic technique as pump-and-probe experiments. In this case, however, the goal is not to study the time evolution of the sample after an excitation, but to study the sample under extreme conditions in a quasi-static excited state that can be maintained only during a short period. This is precisely the case of samples under high pulsed magnetic fields. One of the principal difficulties is related to the synchronization of the detection: the detector must integrate X-ray photons only during the maximum of the magnetic pulse. In general, this is usually done either by using a mechanical X-ray chopper (see, for example, Wulf *et al.*, 1997) or using electronic gating.

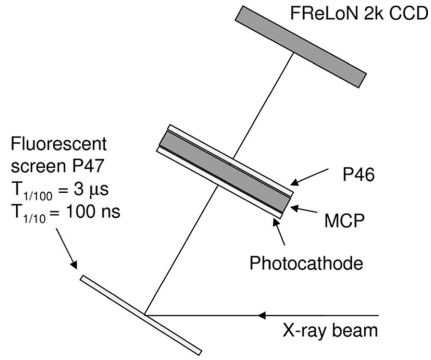

Figure 5
Principle of the CCD camera gating.

With the detection scheme of ID24 based on a CCD camera, we have developed an intermediate solution based on a gating at the level of the visible photons (Fig. 5). The unit is inserted between the fluorescent screen and the FReLoN (fast-readout low-noise) CCD camera. The X-ray converter is a 41 µm-thick P47 phosphor screen with decay times of 100 ns for 10% afterglow and 3 µs for 1% afterglow. The gated unit is a 25 mm-diameter multichannel-plate (MCP) image intensifier with 100 ns minimum gating time from Proxitronic. The image intensifier is coupled to the phosphor screen and to the CCD camera by a high-aperture tandem lens systems. The resulting input field width is 51 mm, with 25 µm pixel pitch. The effective spatial resolution (line-spread function FWHM) is of the order of 200 µm, mainly limited by the image intensifier. The gating is achieved by controlling the high voltage applied on the photocathode. Variable gating down to 16 ns could be used and applied at a frequency up to 16 kHz.

The CCD camera on ID24 is version 2000 of the FReLoN 2k CCD camera. The FReLoN detector is a versatile CCD camera developed at the ESRF. Main characteristics combine low noise, high dynamic range, high readout speed and an improved duty cycle. Technical details of the camera can be found elsewhere (Labiche *et al.*, 2007). For 'pseudo time-resolved' applications, ID24 is particularly interested in the possibilities offered by the FReLoN camera and its control system: (i) quick readout of only the part of the chip exposed to X-rays, leading in our configuration to a dead time (shifting time + readout time) as small as 0.8 ms; (ii) repetition of this cycle with a quasi infinite number of frames ('kinetic pipeline mode'); (iii) very precise control of the timing at ± 12 ns (input/output of the exposure time, readout time, and shutter closing time through the rear panel of the camera).

The timing capabilities of the whole system (gating + CCD camera) has been tested in the four-bunch filling mode of the machine where four equally spaced electron bunches are stored in the synchrotron ring. This leads to an X-ray time structure consisting of regular bunches every ~ 0.7 µs. The MCP gating was synchronized with the arrival of X-ray bunches through the RF signal provided by the machine. The basic frequency of the RF signal (352 kHz) was divided by 352 to lead to a repetition rate of 1 kHz. The gating was kept open

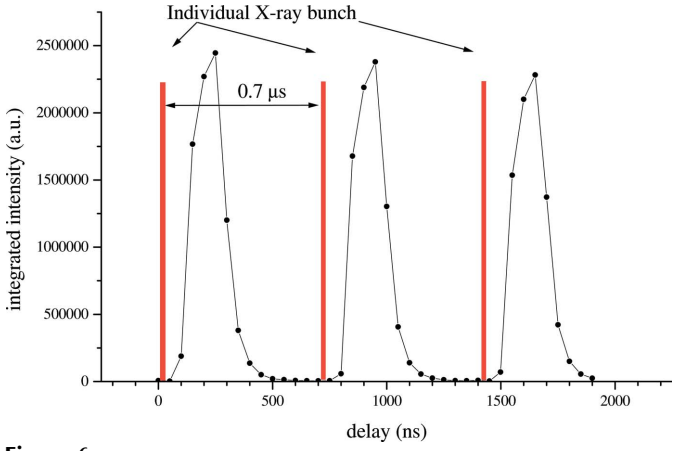

Figure 6
Performance of the CCD camera gating system. Vertical lines symbolize the arrival of the single X-ray bunch.

for 100 ns while the CCD camera was integrating continuously. A variable delay between the arrival of the X-ray bunch and the gating was scanned through 2000 ns. Fig. 6 presents the integrated intensity of the CCD camera *versus* this delay. The vertical lines symbolize the arrival of single X-ray bunches. It demonstrates that the system is able to separate single X-ray bunches in the ESRF four-bunch filling mode. The width of each pulse (FWHM = 180 ns) is larger than the real width of the X-ray bunches (100 ps) and is due to the decay time of the P47 first fluorescent screen ($1/e$ = 100 ns). This gating system is thus suited to the pulsed magnetic field application.

3.4. Synchronization of the magnetic field with the detection

The timing of the coil power supply cannot be controlled and repeated precisely owing to non-constant charging time of the capacitor, and thus the synchronization of the pulsed magnetic field with the detection is triggered by the magnetic discharge itself through a constant fraction discriminator (CFD). Two pick-up coils are set inside the main coil and provide the dB/dt calibrated signal allowing the applied magnetic field to be measured with 2% accuracy. At the beginning of the pulse, the dB/dt signal exhibits a very sharp rising edge. As the delay between this edge and the maximum of the field is constant, we used this signal to trigger the detection. Fig. 7 presents a principle diagram of the synchronization between the magnetic field and the detection. For every single magnetic pulse, all signals are monitored and stored to check for any synchronization problems.

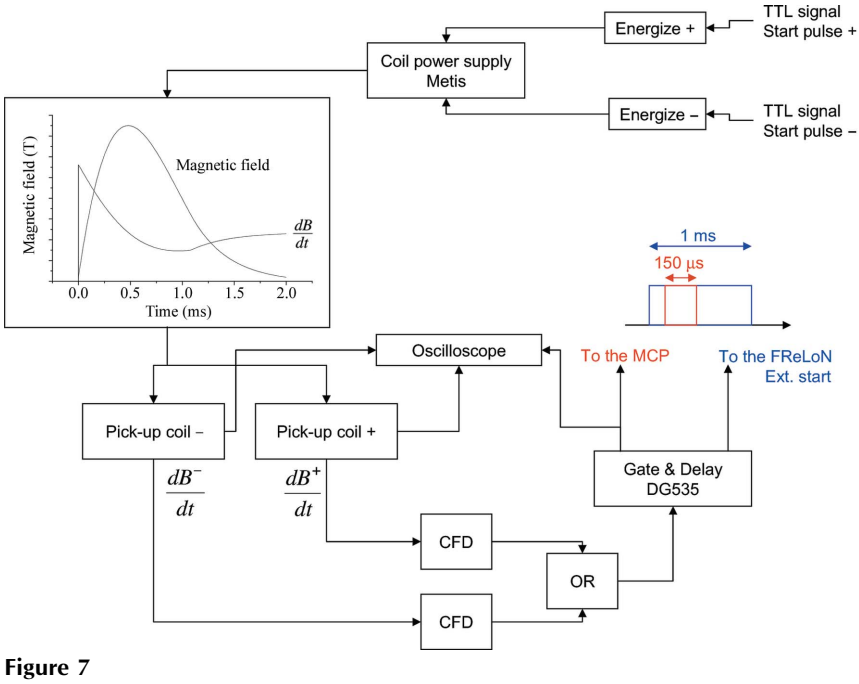

Figure 7
Synchronization principle of the detection and of the pulsed magnetic field.

3.5. Measurement procedure

The XMCD signal is defined as follows,

$$\mathrm{XMCD} = \mu^{\mathrm{L}} - \mu^{\mathrm{R}} = \ln\left(I_0^{\mathrm{L}}/I_1^{\mathrm{L}}\right) - \ln\left(I_0^{\mathrm{R}}/I_1^{\mathrm{R}}\right),$$

where μ^{L} and μ^{R} are the X-ray absorption coefficients measured using left and right circular polarization (LCP and RCP).

In order to reduce systematic errors, we record the four symmetry cases of the XMCD signal obtained by flipping the helicity of the incoming photons (RCP/LCP) and the magnetic field +/−, and average over a large number of repetitions, as explained by Mathon *et al.* (2004*a*). The coil power supply and the synchronization scheme allow a +/− magnetic field to be applied indifferently through a TTL signal. The measurement sequence is in general the following: RCP field +, RCP field −, LCP field −, LCP field +. The XMCD signals are then calculated independently for the two RCP and LCP cases. Taking the average of these two measurements greatly reduces systematic errors and highlights the magnetic origin of the calculated signal.

The measurement sequence includes temperature control of the coil and of the sample, and also a check of safety and amplitude parameters of the magnetic shot. An example of the whole sequence for RCP and field + is presented on the diagram shown in Fig. 8.

4. XMCD at the Re L_2 and L_3 edges in the double perovskite Sr_2CrReO_6

The pulsed-field XMCD set-up has been commissioned with measurements of dichroic spectra *versus* applied magnetic field and temperature at the Re L_2 and L_3 edges of a Sr_2CrReO_6 powder sample. This compound belongs to the family of double perovskites which are being actively studied owing to their promising magnetoresistive properties and high Curie temperature. A review of these compounds has been recently published (Serrate *et al.*,

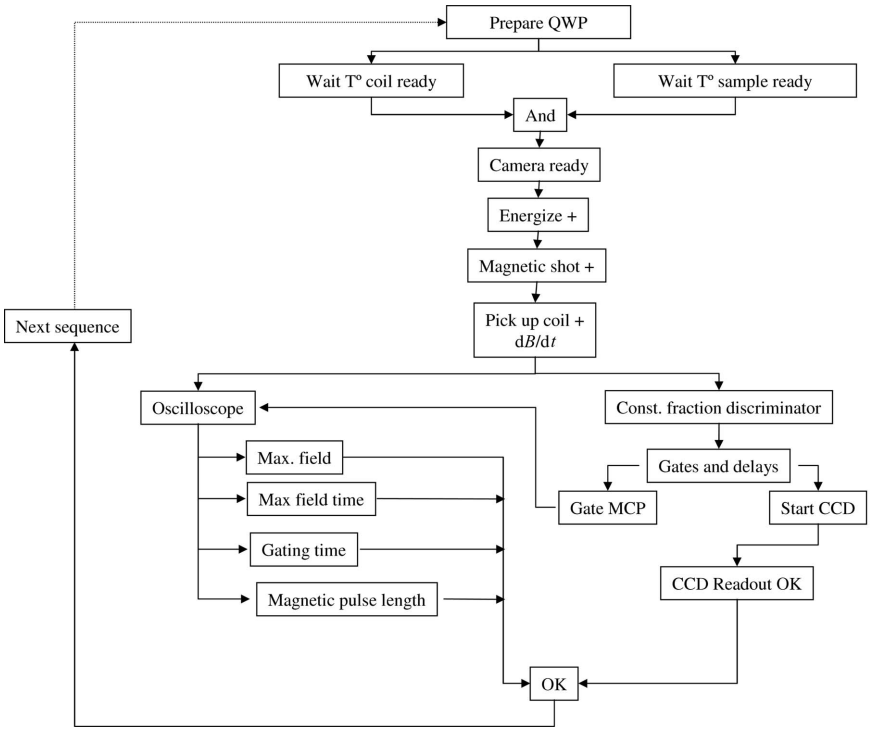

Figure 8
Typical XMCD measurement sequence.

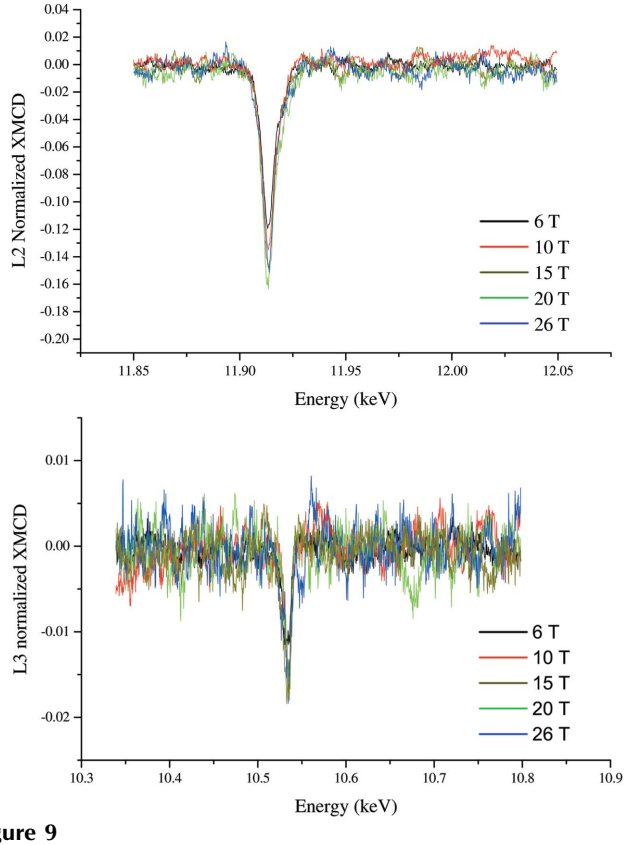

Figure 9
XMCD spectra recorded at the Re L_2 (top) and L_3 (bottom) edges on the double perovskite Sr_2CrReO_6 under various applied magnetic fields and T = 5 K.

2007). Sr_2CrReO_6 exhibits a very high Curie temperature (635 K), which makes it a promising candidate for spintronic applications at room temperature (Kato *et al.*, 2002). The high Curie temperature in this compound has been accounted for by suitable band matching and structural properties (De Teresa *et al.*, 2005). The extraordinary properties of the compound arise from half-metallicity, *i.e.* only one spin direction being populated in the conduction band, which consists of overlapping spin-down Cr(3*d*), O(2*p*), Re(5*d*) electronic bands. Another remarkable property of this compound is the strong magnetic anisotropy arising from significant spin–orbit coupling at Re atoms, which brings about an unquenched Re orbital moment (Michalik *et al.*, 2007). Recent XMCD measurements performed at room temperature under a steady field of 6 T revealed strong negative signals with amplitudes of 14% and 2.5% at the Re L_2 and L_3 edges, respectively (Majewski *et al.*, 2005), which can be detected with sufficient statistics within the short effective acquisition time of the pulsed technique.

Fig. 9 presents the measured XMCD spectra and demonstrates clearly the feasibility of such an experiment on a dispersive-XAS beamline. The overall increase of the XMCD amplitude *versus* applied field from 6 to 26 T by ∼10% reproduces that of the bulk sample magnetization (Michalik *et al.*, 2007; De Teresa *et al.*, 2007), indicating correct control of the applied field (integration times). We have also performed temperature-dependent measurements at the Re L_2 edge under a field of 26 T; the spectra obtained are presented in Fig. 10. The amplitude of the XMCD signal qualitatively follows the temperature dependence of the bulk magnetization. A complete analysis of the results will be reported elsewhere (Sikora *et al.*, 2007). At 26 T, a good signal-to-noise

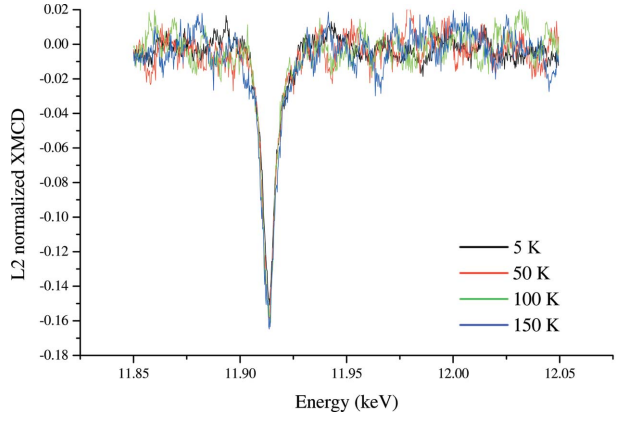

Figure 10
XMCD spectra recorded at the Re L_2 edge on the double perovskite Sr_2CrReO_6 at various temperatures and an applied magnetic field of 26 T.

ratio was obtained with a total of 200 magnetic pulses corresponding to 5 h of experiment and to 60 ms of cumulated integration time. With the optimized version of the coil, the same signal-to-noise ratio can be obtained in 24 min.

5. Concluding remarks

For the first time we demonstrate the possibility of recording high-quality XMCD spectra under high magnetic fields on the ID24 energy-dispersive XAS beamline of the ESRF. Using a new sample environment as well as a dedicated detection system, both developed by the ESRF, XMCD spectra have been recorded under high magnetic fields up to 26 T and low temperatures down to 5 K. We show results relative to a first demonstration experiment at the Re L_2 and L_3 edges of the double perovskite Sr_2CrReO_6. The sample environment developed by the ESRF is able to deliver pulses with field strengths up to 30 T.

Further developments will include an increase in the applied magnetic field up to 40 T and an improvement of the measurement duty cycle.

The authors would like to acknowledge the work of the technical and engineering team of the sample environment support service, the detector system group and the beamline ID24 technical and engineering staff that makes these experiments possible: J. Jacobs, C. Jarnias, M.-C. Dominguez, S. Pasternak, A. Rodriguez and F. Perrin. We acknowledge the European Synchrotron Radiation Facility for provision of beam time through the peer-reviewed project MI739 and in-house research time.

References

Altarelli, M. (1993). *Phys. Rev. B*, **47**, 597–598.
Ankudinov, A. L. & Rehr, J. J. (1995). *Phys. Rev. B*, **51**, 1282–1285.
Bonfim, M., Mackay, K., Pizzini, S., San Miguel, A., Tolentino, H., Giles, C., Neisius, T., Hagelstein, M., Baudelet, F., Malgrange, C. & Fontaine, A. (1998). *J. Synchrotron Rad.* **5**, 750–752.
Carra, P., Thole, B. T., Altarelli, M. & Wang, X. (1993). *Phys. Rev. Lett.* **70**, 694–697.
De Teresa, J. M., Michalik, J. M., Blasco, J., Algarabel P., Ibarra, M. R., Kapusta, C. & Zeitler, U. (2007). *Appl. Phys. Lett.* **90**, 252514.
De Teresa, J. M., Serrate, D., Ritter, C., Blasco, J. & Ibarra, M. R. (2005). *Phys. Rev. B*, **71**, 092408.
Frings, P., Vanacken, J., Detlefs, C., Duc, F., Lorenzo, J. E., Nardone, M., Billette, J., Zitouni, A., Bras, W. & Rikken, G. L. J. A. (2006). *Rev. Sci. Instrum.* **77**, 063903.
Giles, C., Malgrange, C., Goulon, J., de Bergevin, F., Vettier, C., Dartyge, E., Fontaine, A. & Pizzini, S. (1994). *Nucl. Instrum. Methods*, A**349**, 622–625.
Hagelstein, M., Fontaine, A. & Goulon, J. (1993). *Jpn. J. Appl. Phys.* **32**(Suppl. 32–2), 240–242.
Hagelstein, M., San Miguel, A., Fontaine, A. & Goulon, J. (1997). *J. Phys. IV*, C**2**, 303–308.
Kato, H., Okuda, T., Okimoto, Y., Tomioka, Y., Takenoya, Y., Ohkubo, A., Kawasaki, M. & Tokura, Y. (2002). *Appl. Phys. Lett.* **81**, 328–330.
Koch, A., Hagelstein, M., San Miguel, A., Fontaine, A. & Ressler, T. (1995). *Proc. SPIE*, **2416**, 85–93.
Labiche, J.-C., Mathon, O., Pascarelli, S., Newton, M. A., Guilera-Ferre, G., Curfs, C., Vaughan, G., Fernandez-Garcia, D. & Homs, A. (2007). *Rev. Sci. Instrum.* Accepted.
Mackay, K., Bonfim, M., Givord, D. & Fontaine, A. (2000). *J. Appl. Phys.* **87**, 1996–2002.
Majewski, J. M. P., Geprägs, S., Sanganas, O., Opel, M., Gross, R., Wilhelm, F., Rogalev, A. & Alff, L. (2005). *Appl. Phys. Lett.* **87**, 202503.
Mathon, O., Baudelet, F., Itié, J.-P., Pasternak, S., Polian, A. & Pascarelli, S. (2004*a*). *J. Synchrotron Rad.* **11**, 423–427.
Mathon, O., Baudelet, F., Itié, J.-P., Polian, A., d'Astuto, M., Chervin, J.-C. & Pascarelli, S. (2004*b*). *Phys. Rev. Lett.* **93**, 255503.
Matsuda, Y. H., Ueda, Y., Nojiri, H., Takahashi, T., Inami, T., Ohwada, K., Murakami, Y. & Arima, T. (2004). *Physica B*, **346–347**, 519–523.
Michalik, J. M., De Teresa, J. M., Ritter C., Blasco, J., Serrate, D., Ibarra, M. R., Kapusta, C., Freudenberger, J. & Kozlova, N. (2007). *Europhys. Lett.* **78**, 17006.
Narumi, Y., Kindo, K., Katsumata, K., Kawauchi, M., Broennimann, C., Staub, U., Toyokawa, H., Tanaka, Y., Kikkawa, A., Yamamoto, T., Hagiwara, M., Ishikawa, T. & Kitamura, H. (2006). *J. Synchrotron Rad.* **13**, 271–274.
Pascarelli, S., Mathon, O. & Aquilanti, G. (2004). *J. Alloys Compd.* **363**, 33–40.
Pellicer-Porres, J., San Miguel, A. & Fontaine, A. (1998). *J. Synchrotron Rad.* **5**, 1250–1257.
Pizzini, S., Bonfim, M., Baudelet, F., Tolentino, H., San Miguel, A., Mackay, K., Malgrange, C., Hagelstein, M. & Fontaine, A. (1998). *J. Synchrotron Rad.* **5**, 1298–1303.
San-Miguel, A., Hagelstein, M., Borrel, J., Marot, G. & Renier, M. (1998). *J. Synchrotron Rad.* **5**, 1396–1397.
Serrate, D., De Teresa, J. M. & Ibarra, M. R. (2007). *J. Phys. Condens. Matter*, **19**, 023201.
Sikora, M. *et al.* (2007). In preparation.
Stöhr, J. (1999). *J. Magn. Magn. Mater.* **200**, 470–493.
Thole, B. T., Carra, P., Sette, F. & van der Laan, G. (1992). *Phys. Rev. Lett.* **68**, 1943–1946.
Trapananti, A. *et al.* (2007). In preparation.
Van der Linden, P. *et al.* (2007). In preparation.
Wulf, M., Schotte, F., Naylor, G., Bourgeois, D., Moffat, K. & Mourou, G. (1997). *Nucl. Instrum. Methods A*, **398**, 69–84.